Journal of Solid State Chemistry 186 (2012) 149–157

Contents lists available at SciVerse ScienceDirect

Journal of Solid State Chemistry

journal homepage: www.elsevier.com/locate/jssc

A novel approach for enhanced visible light activity in doped nanosize titanium dioxide through the excitons trapping

Kanakkanmavudi B. Jaimy, K.V. Baiju [1], Swapankumar Ghosh, K.G.K. Warrier *

National Institute for Interdisciplinary Science & Technology, CSIR, Trivandrum 695019, India

ARTICLE INFO

Article history:
Received 14 July 2011
Received in revised form
30 November 2011
Accepted 30 November 2011
Available online 8 December 2011

Keywords:
Sol–gel growth
Optical properties
Phase transition

ABSTRACT

Titanium dioxide doped with iron oxide (0–10 mol%) has been synthesized by an aqueous sol–gel method. The extent of phase transformation is higher in presence of up to 1 mol% of Fe^{3+} ions in doped titania. A further increase in Fe^{3+} content was found to decrease the phase transformation. A composition which contains ~90% rutile and the remaining anatase phase shows the highest photocatalytic activity. Even though surface area values are dramatically decreased by the modification of TiO_2 by Fe^{3+} doping, crystallinity plays a major role in photocatalytic activity enhancement. UV–vis reflectance spectra indicate a red-shift in band gap energy and thus an enhanced photoactivity in visible light, suitable for application in photodegradation of toxic industrial effluents as well as other organic contaminants, is achieved. Low concentrations of Fe^{3+} ions act as excitons trapping centers, while higher concentrations act as recombination centers. The synergy between the rutile–anatase ratios and optimum amount of Fe^{3+} ions improve the interfacial charge transfer and trapping which enhanced the photochemical degradation of MB dye. The Fe^{3+} doped TiO_2 composition has the highest photoactivity, having an apparent rate constant of 11.1×10^{-3} min^{-1}, which is much higher than that of commercial P25 Degussa titania (6.03×10^{-3} min^{-1}).

1. Introduction

Titanium dioxide, commonly named as titania, comes under the broad umbrella of ceramic semiconductors, which have increasingly been employed in the area of photocatalysis [1]. An ideal photocatalyst should be chemically and biologically inert, become significantly activated by sunlight, possess the ability to catalyze reactions, remain stable and be nontoxic to the environment while decomposing hazardous industrial wastes [2,3]. Titanium dioxide is close to being an ideal photocatalyst, displaying almost all of the above properties. However, its practical application seems limited due to its wide band gap [3.0–3.2 eV], which corresponds to the absorption in UV region (3–5%) of the solar spectrum [4]. To use the solar spectrum efficiently, titania should be activated in the visible light region [5,6]. The three main approaches reported for the synthesis of visible light activated titania are: (i) doping with anions of B, C, S, N and F [7–11], (ii) coupling with a semiconductor which absorbs visible light [12] and (iii) doping with Cr^{3+}, V^{3+} and similar metal ions [13,14]. Noble metals are usually introduced into TiO_2 for enhancing visible light photocatalytic activity [15]. Litter and Navio [16] proposed a mechanistic effect of Fe^{3+} in titania during photocatalysis and the spectral response upon Fe^{3+} addition was studied by Bockelmann et al. [17]. Photocatalytic activity of TiO_2 is influenced by the crystal structure (anatase, rutile), surface area, porosity, surface charge density, particle size and its distribution. Increased photocatalytic activity is reported for powders with high anatase/rutile ratio, low crystallite size, high surface area and porosity [18]. Small anatase crystals with high surface area and high porosity are good photocatalysts. Recent studies have indicated, however, that a mixed phase of anatase and rutile display much higher photocatalytic activity compared to either anatase or rutile alone. Ohno et al. [19] proposed a synergistic effect of anatase and rutile in support of the enhanced photocatalytic activity.

Numerous synthetic approaches including high energy ion implantation [20], flame spray pyrolysis [21] and sol–gel methods [22] are reported on the synthesis of doped nanostructured titania. The majority of the sol–gel methods utilize alkoxide precursors as the starting materials. A facile aqueous route [23] was utilized for preparing photoactive titanium oxide from titanylsulfate. The visible light photocatalysts other than TiO_2, such as Bi_2WO_6, also show better activity (the highest NO removal rate of 110 ppb min^{-1}), in the as prepared catalyst [24]. However, in this

* Corresponding author. Fax: +91 471 249712.
E-mail address: wwarrierkgk@yahoo.co.in (K.G.K. Warrier).
[1] *Present address*: Centre for Materials for Electronics Technology (C-MET), Department of Information Technology, Kerala-680581, India.

0022-4596/$ - see front matter © 2011 Elsevier Inc. All rights reserved.
doi:10.1016/j.jssc.2011.11.052

work, the visible light activity achieved is higher for powders calcined at 800 °C. Commercial glazed tiles, coated with TiO_2 precursor sols and annealed at 700–800 °C, have been found to be photoactive [25].

Though there are a few reports [26,27] on Fe doped sol–gel synthesized TiO_2 catalyst with enhanced visible photocatalytic activity, there is no proper explanation for the enhancement of the activity in visible light. Fe(III) oxides have the advantage of low cost compared to noble metals. In the present work, we report a systematic approach to synthesize nanosized iron(III) doped titania by a simple aqueous sol–gel method using titanylsulfate. The structural modifications in titania as a result of doping and subsequent thermal treatment are investigated using X-ray diffraction (XRD) and HR-TEM. The photocatalytic activity of the TiO_2 catalyst was studied by monitoring the degradation of aqueous suspension of Methylene Blue (MB) dye. An attempt is made now to explain the synergy and mechanism of enhanced photoactivity. The results reported indicate the possibility that titania doped with iron oxide could be a promising photocatalyst under visible light.

2. Experimental

2.1. Chemicals

Titanylsulfate (98%, M/s Travancore Titanium Products, Trivandrum, India), ammonium hydroxide solution (25%, s.d. FINE-CHEM Ltd, India), HNO_3 (Merck, India), Fe(III) nitrate heptahydrate (Analytical Grade, s.d. FINE-CHEM Ltd, India), Methylene Blue dye (Analytical Grade, Qualigens Fine Chemicals, India) and Degussa P25 commercial titanium dioxide. All the chemicals were used as received without any further purification.

2.2. Synthesis of Fe^{3+} doped TiO_2 sol by aqueous sol–gel method

Titanylsulfate was used as the precursor for the preparation of nano titanium oxide. In a typical experiment, titanylsulfate (~16.2 g) was dissolved in 500 mL of distilled water and hydrolyzed by adding ammonium hydroxide solution (25%) under constant stirring, until the pH of the precipitate was 7.5. The precipitate formed was separated by filtration and washed with distilled water until free from sulfate ions by the $BaCl_2$ test. In order to produce a stable titania sol, the precipitate was dispersed in 1 L hot distilled water and was peptized by adding HNO_3 (1.5 M) solution until the pH was 1.7–2. Calculated volumes of 0.5 M Fe(III) nitrate solution were added drop wise to the titania sol under constant stirring which was continued for 3 h for stabilizing the sol. Doped titania sols were synthesized with Fe^{3+} dopant concentrations 0, 0.125, 0.25, 0.5, 0.75, 1, 2, 5 and 10 mol% and are referred as T and TF*x* where *x* is the Fe^{3+} content (mol%). Dry gels were annealed at varying temperatures (600, 700, 800 and 900 °C) with 1 °C min^{-1} ramp and 1 h exposure time. The calcined powders were characterized by various techniques.

2.3. Characterization

X-ray diffraction (XRD) patterns of calcined powders were taken in X'pert PRO, Philips, Diffractometer, in the 2θ range 20–60° using Cu$K\alpha$ radiation. The crystallite size was calculated using the Scherrer formula [28] as given in equation

$$D_{XRD} = k\lambda/\beta \cos\theta \quad (1)$$

where D_{XRD} is the average crystallite size (nm), k, the shape factor, λ is the X-ray wavelength (1.5406 Å), β is the full width at half maximum (in radian) of (1 0 1) peak and θ is the Bragg angle. The amount of rutile in the calcined samples was estimated using the Spurr equation [29]

$$F_R = \frac{1}{[1+\{0.8I_A(101)/I_R(110)\}]} \quad (2)$$

where F_R is the mass fraction of rutile in the sample and I_A (1 0 1) and I_R (1 1 0) are the integrated main peak intensities of anatase and rutile, respectively. Fourier transform infrared (FTIR) spectra were recorded in a Magna 560, Nicolet, Madison, Wisconsin spectrophotometer in the 4000–400 cm^{-1} range on powder samples dispersed in KBr pellets. The reflectance spectra of the calcined powders were obtained using a UV–visible 2401 PC spectrophotometer (Shimadzu) in the 200–800 nm range. The band gap energy was calculated by Tauc plot method. The Kubelka–Munk function, $f(R)$, was considered proportional to the absorption of radiation and band gap energy, 'E_g (in eV)' of the semiconductor. The function $f(R)$ was calculated using the equation

$$f(R) = (1-R)^2/2R \quad (3)$$

The band gap energies (E_g) were obtained from the intersection of the linear regression of fast decay zone of $f(R)$ spectrum to the energy axis of $(f(R)h\nu)^{1/2}$ versus $h\nu$ plot [25].

The crystal structure and particle size of calcined titania powders were determined from HR-TEM using a FEI Tecnai G^2 30 S-Twin HR-TEM equipped with a Gatan CCD camera and operated at 300 kV. BET surface area measurements were carried out by nitrogen adsorption at 77 K using a Micromeritics Gemini 2375 surface area analyzer after degassing the samples at 200 °C for 2 h. Average pore diameters were derived from the N_2 adsorption–desorption isotherms by the BJH method. The photoluminescence (PL) spectra, obtained at an excitation wavelength of 320 nm, were recorded on a Spex-Fluorolog FL22 spectrofluorometer equipped with a double grating 0.22 m Spex 1680 monochromator and a 450 W Xe Lamp as an excitation source operating in the front face mode.

2.4. Measurement of photocatalytic activity

The visible light photocatalytic activity of calcined powders was studied by monitoring the degradation of Methylene Blue (MB) dye in an aqueous suspension containing pure and Fe^{3+} doped nanocrystalline TiO_2 under visible light exposure with constant magnetic stirring. As the decolorization of MB involves just two electron transfer from photocatalyst to MB which leads to the complete disappearance of its visible light absorption due to the formation of MBH2, MB degradation may not be a real measure of catalytic activity. However, selection of MB as a model dye in this work was done on the basis of many reports [26,30,31] which have used MB for measuring the photocatalytic activity. Approximately 0.1 g titania powder, dispersed in 100 mL water, was mixed with an aqueous solution of MB (1.25×10^{-5} M). The suspension was stirred in the dark for 30 min to allow adsorption of MB dye, if any, by the nanocrystalline TiO_2 powders. The titania suspension was subsequently exposed to visible light of 398–800 nm wavelength with an intensity of 7 mW cm^{-2} using a 1000 W mercury lamp. Three UV filters were used to eliminate UV radiation, if any, in the emitted light. After each exposure, ~5 mL suspensions were taken out from the irradiation chamber at time intervals of 20, 40, 60, 80, 100 and 120 min. The powder was separated out of the suspension using a table top centrifuge at 3000 g rcf. The filtrate was then examined using a UV–visible spectrometer, to study the degradation of the aqueous MB solution in visible light. The absorption spectra of the MB dye solution were obtained in the 200–800 nm range. The absorption maximum at 663.2 nm in the spectrum of Methylene Blue was

used to determine the concentration. The initial absorbance (A_0) was obtained from the UV–vis spectrum of the MB suspension, stirred in the dark and without the visible light exposure and was taken as the initial MB dye concentration (C_0). The absorbance (A) of MB solutions, after irradiation time intervals of 20, 40, 60, 80, 100 and 120 min, was taken as a measure of the residual concentration, C, of MB dye. The efficiency of degradation was calculated from the equation

$$C/C_0 = A_{t=t}/A_{t=0} \quad (4)$$

where $A_{t=0}$ is the initial absorbance of MB solution and $A_{t=t}$ is the absorbance values after the fixed time intervals. The photocatalytic decomposition of the organic molecules follows the Langmuir–Hinshelwood kinetics [30], which may be represented as equation (Eq. (5)).

$$dC/dt = k_{app}C \quad (5)$$

where 'dC/dt' represents the rate of change in the MB dye concentration with respect to the irradiation time 't', 'k_{app}' the apparent first-order reaction rate constant and 'C' the concentration of the MB dye. Ln C_0/C was plotted against time of visible light exposure. k_{app} was obtained from the slope of the linear regression of ln C_0/C versus exposure time plot. A control experiment was performed with MB dye solution in the absence of photocatalyst powder. The initial MB dye concentration remained unchanged even after irradiating the sample for total 2 h. Commercially available Degussa P25 (~70% anatase) TiO_2 was also irradiated under the identical conditions to compare the photocatalytic activity.

3. Results and discussion

3.1. Structural characterization

X-ray diffraction analysis data of TiO_2 with different concentrations of Fe^{3+} doping, annealed at 800 °C, presented in Fig. 1 show that there is a gradual decrease in anatase phase content in doped TiO_2 with the increase in Fe^{3+} doping from 0 to about 1 mol%, followed by a steady increase up to 10 mol%. Peaks corresponding to α-Fe_2O_3 and Fe_2TiO_4 are not observed in any of the XRD data and it may be due to the fact that all the Fe^{3+} ions were incorporated into the structures of titania and replaced the Ti^{4+} ion or alternatively they have entered at the interstitial sites [4]. In pure titania, ~65% anatase is present even after calcination at 800 °C. However, this is reduced to 10% in TF0.25.

On calcination at 800 °C, titania doped with 1 mol% Fe^{3+} completely transformed to rutile phase by reducing the surface energy required for the formation of critical nuclei of the rutile phase [32]. The anatase content then slowly increased almost linearly to ~18% for the 10 mol% Fe^{3+} addition. Increasing the Fe^{3+} concentration beyond an optimum level acts as "second phase stabilizer" in the TiO_2 matrix. The number of intergranular contacts and contact area among titania grains will decrease upon increased addition of iron oxide which inhibits grain growth [32,33]. Critical size of rutile nuclei is not reached by the grain growth inhibition and this reduces the rutile phase formation. There is an initial increase in anatase crystal diameter (D_{XRD}) when pure titania is doped up to ~0.25 mol% Fe^{3+} (Fig. 1B) and beyond that a gradual decrease at all temperatures and this is due to the restriction of grain growth by the iron oxide barrier among the grains [34].

The variation of the lattice parameters 'a' and 'c' of the rutile phase (TiO_2 calcined at 800 °C) with different concentrations of Fe^{3+} ions are presented in Fig. 2. The ionic radii of Ti^{4+} (0.68 Å) and Fe^{3+} (0.64 Å) are almost equal for co-ordination number 6,

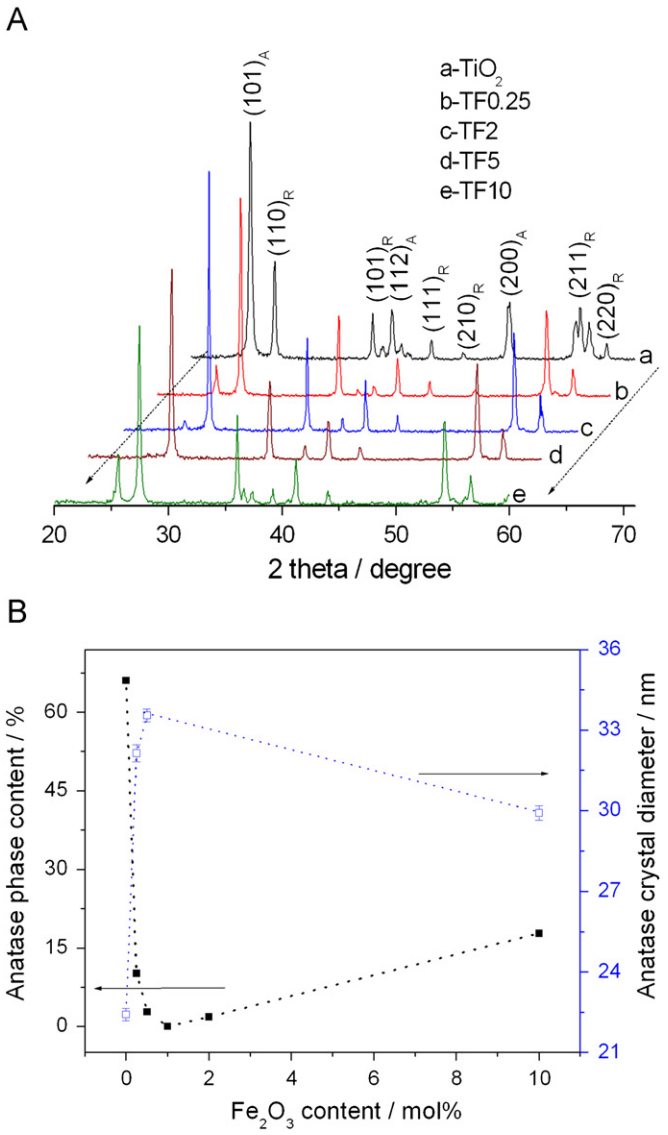

Fig. 1. (A) X-ray diffraction patterns of pure and Fe^{3+} doped titania powders and (B) comparison of amount and crystallite size of anatase phase versus Fe^{3+} dopant concentrations in TiO_2, calcined at 800 °C.

making it easy for Fe^{3+} to be substituted in the position of a Ti^{4+} in TiO_2 lattice.

By increasing the concentration of Fe^{3+} ions, lattice parameters 'a' and 'c' showed a small but steady decrease. Fe^{3+} ions can easily fit into the titania lattice, especially in the rutile form due to its open channel structure [35]. The slight distortion observed in the rutile structure suggests the formation of a solid solution of Fe^{3+} in the titania matrix [35]. Through the addition of Fe^{3+}, the anatase to rutile phase transformation is enhanced at all temperatures.

FTIR spectra of T, TF0.25 and TF10 compositions, calcined at 800 °C, are presented in Fig. 3. A broad band between 3600 and 3050 cm^{-1}, centered around 3400 cm^{-1}, indicates the presence of an –OH group (O–H stretching vibrations) on the surface of the gel and the band around 1630 cm^{-1} indicates the presence of molecularly adsorbed water (H–O–H bending vibrations) in the gel [27]. A small band centered around 1390 cm^{-1} is due to N–O stretching vibrations, indicating the presence of NO_3^- ions [36]. Peaks below 1000 cm^{-1} correspond to Ti–O and Ti–O–Ti bending vibrations [37]. The surface hydroxyl groups are important in photocatalysis and TF0.25 sample shows predominant bands for –OH group. Hydroxyl groups are major hole scavengers, and

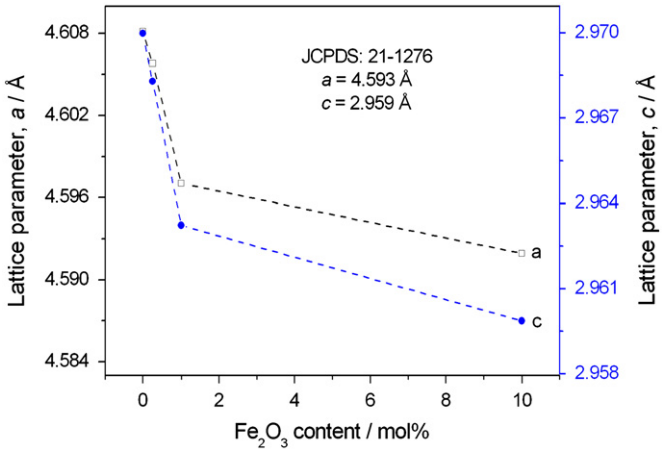

Fig. 2. Variation of lattice parameters '*a*' and '*c*' of rutile in doped titania composites, calcined at 800 °C, as a function of Fe^{3+} concentration.

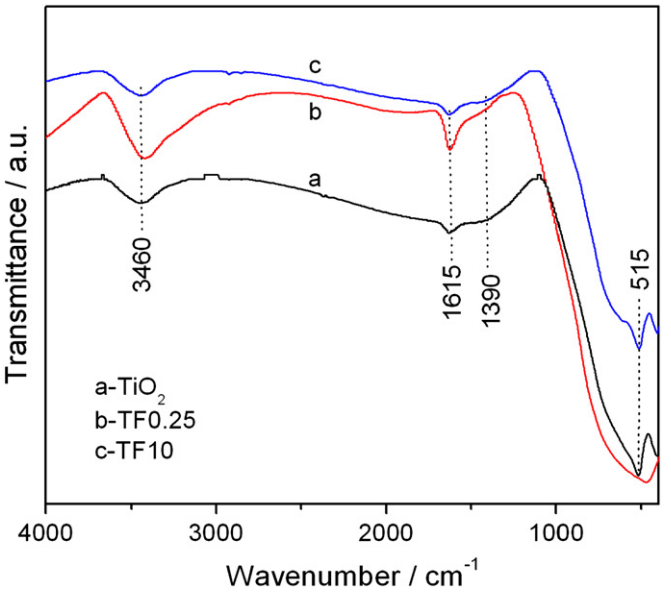

Fig. 3. Fourier transform infrared spectra of pure and Fe^{3+} doped titania powders, annealed at 800 °C.

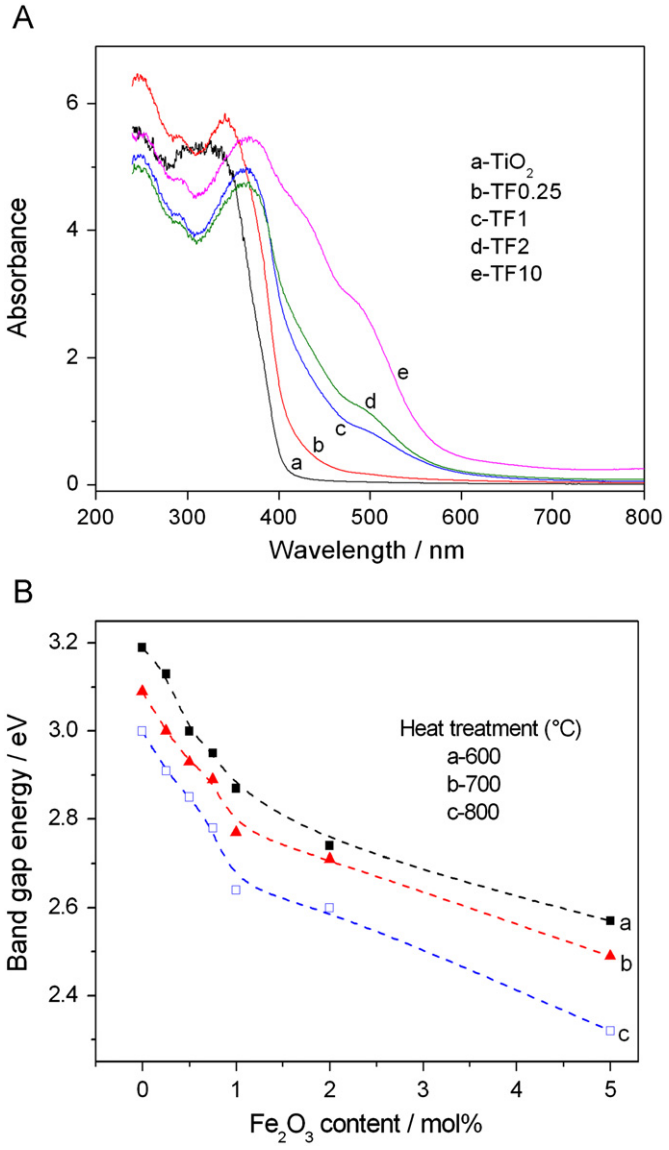

Fig. 4. (A) Comparison of absorbance plots of pure and Fe^{3+} doped titania annealed at 800 °C. (B) Variation in band gap energy of titania with Fe^{3+} concentration, samples calcined at various temperatures.

this may help in the enhanced photocatalytic activity of doped composition.

The absorbance spectra of TiO_2 compositions, calcined at 800 °C and the band gap energies (E_g) of pure and doped titania were calculated from UV–vis diffuse reflectance spectra plotted as the Kubelka–Munk function (F) for powders, calcined at different temperatures and are presented in Fig. 4. The absorption edges shift towards longer wavelength for Fe^{3+} doped samples and this indicates a decrease in band gap energy. The band gap energies for pure anatase and the rutile phase are ~3.2 and ~3.0 eV, respectively.

The minimum band gap energy of ~2.3 eV was recorded in the sample TF5, calcined at 800 °C. A significant red-shift has been observed with increasing calcination temperature for all TiO_2 samples at all dopant levels. This may be due to an increase in crystallinity with increase in annealing temperatures, resulting in the formation of new energy bands in semiconducting titania. The absorption shifted from 387 to 540 nm corresponding to the band gap energy (3.2–2.3 eV). Fe^{3+} forms impurity levels in between the valence and conduction bands of titania [35]. The *d*-orbital of the Fe^{3+} ion may overlap with the conduction band of titania and thus the band gap is reduced. A charge-transfer takes place between the 3*d*-electrons of Fe^{3+} and the conduction band of titania [38], resulting in the photoactivation of Fe^{3+} doped titania compositions in the visible light region of the electromagnetic spectrum.

The room temperature photoluminescence (PL) spectra of pure and Fe^{3+} doped nanocrystalline TiO_2 annealed at 800 °C are presented in Fig. 5. Upon doping with Fe^{3+}, the luminescence spectra showed a sharp decrease in intensity. When valence electrons are excited to the conduction band, they can easily be trapped by surface defects at the grain boundaries between nanocrystallites. These excited electrons then interact with the holes at the valence band through radiative or non-radiative pathways and in TiO_2 nanoparticles, the charge-carrier recombination path is non-radiative. For the undoped TiO_2 powder, it shows a band at 417 nm (2.98 eV) in association with the recombination of e^-/h^+ pairs [31]. In Fe^{3+} doped TiO_2, Fe^{3+} cations create surface states of different surface energy levels [39]. These surface states have lower energies than that of the conduction band of TiO_2 and excited electrons can jump in to these levels. Consequently, the excitons' lifetimes are increased, resulting in a quenched PL intensity [15].

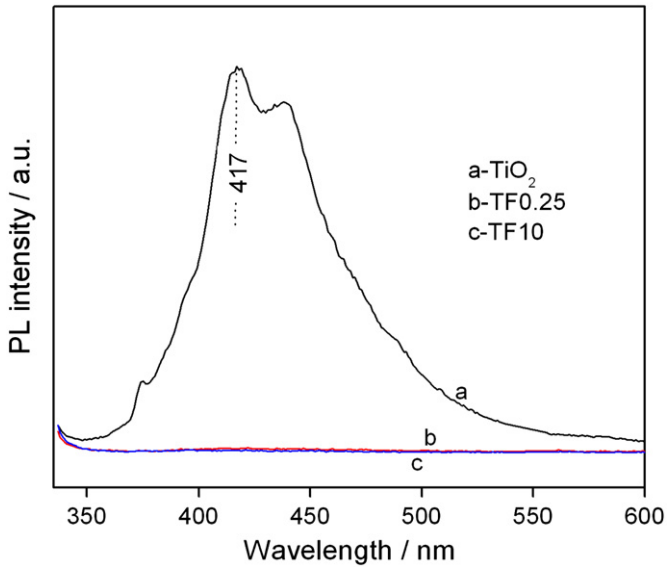

Fig. 5. Photoluminescence spectra of pure and Fe^{3+} doped titania compositions, all calcined at 800 °C.

Another important parameter which influences photocatalysis is surface area. The specific surface area (BET) as well as the pore diameter as a function of Fe^{3+} dopant concentration in TiO_2 and adsorption–desorption isotherms of TF0.25 powder calcined at different temperatures, is shown in Fig. 6. BET surface area was found to decrease with increasing iron concentration as well as calcination temperatures in the doped titania compositions (Fig. 6A). The average pore sizes for all compositions increased with an increase in calcination temperature and Fe^{3+} content due to the increase in crystallite size. A decrease in S_{BET} is due to the collapse of the porous structure at higher temperatures leading to particle coarsening [26]. The collapse of the porous structure also causes pore coalescence at high temperatures resulting in a higher pore diameter compared to undoped counterparts. Adsorption–desorption isotherms of TF0.25 calcined at different temperatures (Fig. 6B) exhibited typical type IV behavior with a hysteresis loop caused by capillary condensations within the mesopores.

The crystal structure and dimensions also decide the photocatalysis and are easily identified by TEM micrographs. The bright field high resolution transmission electron microscopy (HR-TEM) images of TiO_2 calcined at 600 °C (T600) and doped TiO_2 (TF0.25) calcined at 800 °C are presented in Fig. 7. All the samples are highly crystalline, which is evident from the clear crystal facets and sharp SAED patterns in the inset. The HR-TEM image of sample T600 (Fig. 7A) shows lattice fringes corresponding to (101), and (004) planes of anatase with respective interplanar spacing of 0.352 and 0.238 nm, respectively. The SAED pattern for T600 also indicates the sharp diffraction patterns of anatase phase only and this is also supported by X-ray data (not shown here). The particles seen in T600 are single crystals of anatase in the size range 9–12 nm.

The calculated average size (D_{TEM}) on 100 particles from multiple TEM images for T600 is ~10.8 nm which is very close to the crystal diameter of ~12 nm calculated from XRD. Large particles of size ~100 nm in the image correspond to the majority phase, rutile (Fig. 7B, C), and are also single crystals. The smaller particles ~30 nm belong to the ~10% anatase phase. A high resolution image of a square portion of a large particle of TF0.25 calcined at 800 °C (marked in the Fig. 7C) is provided in Fig. 7D where very sharp lattice fringes corresponding to (110) plane with an interplanar spacing of 0.325 nm for rutile are observed.

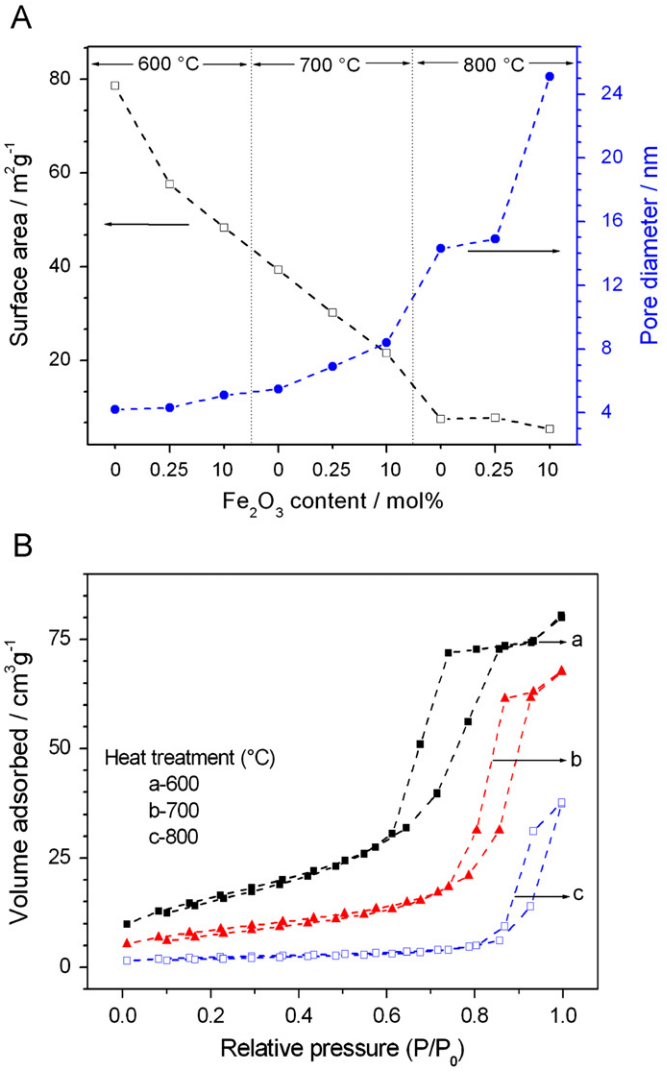

Fig. 6. (A) Variation of BET surface area (empty square) and pore diameter (filled circle) as a function of dopant concentration in TiO_2 and (B) adsorption–desorption isotherms of TF0.25 powder calcined at different temperatures.

3.2. Photocatalytic degradation of Methylene Blue

Photocatalytic behavior of Fe^{3+} doped titania was studied by monitoring the degradation of an MB dye solution. The absorbance curves and degradation of MB dye as a function of light exposure time for pure and doped TiO_2 are depicted in Fig. 8. The Fe^{3+} doped (0.25–1 mol%) TiO_2 compositions are seen to possess higher activity than that of Degussa P25. TF0.25 showed the highest photocatalytic activity and was able to decompose MB completely in about 180 min. While 73% degradation was observed with TF0.25, it only degraded by 43% in the case of undoped titania and 54% for Degussa P25 after 120 min of light exposure. The visible light photocatalytic activity of TF compositions from some published data are shown in Table 1.

Rhodamine is an amino dye and all others containing an azo group and hence the comparison of present work with these reports is relevant. Comparing with the reported results, aqueous sol–gel doped titania has potential for faster decolorization and is more effective for higher temperature operations. Simplicity of synthetic method and inexpensive precursors are the major advantages with the doped photocatalyst reported here. The variation in the visible light photocatalytic rate constants, k_{app}, as a function iron oxide and rutile content in doped titania

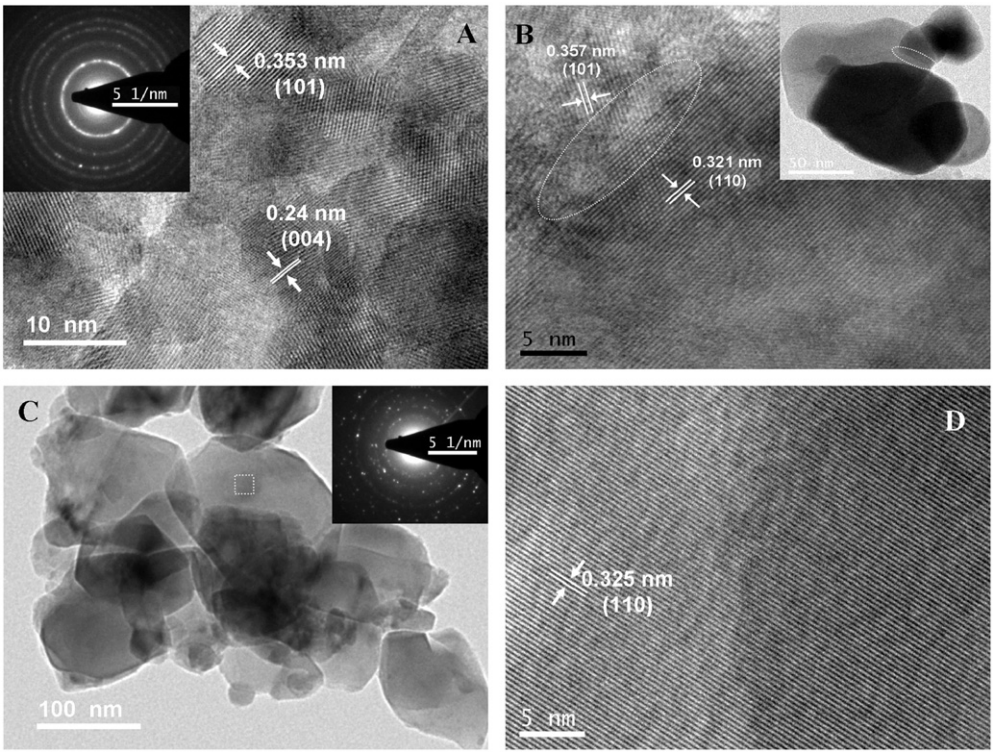

Fig. 7. HR-TEM images of titania (A) T600 with anatase single crystals with average size of ~10.8 nm showing (101) and (004) lattice planes. The SAED pattern of the same is shown in the inset, (B) TF0.25 calcined at 800 °C consisted of both anatase and rutile crystals showing the interface between them in the marked region, (C) TF0.25 calcined at 800 °C with its SAED pattern in the inset and (D) high resolution image of a small region (dotted square) of one of the large rutile particles from (C) with (110) lattice fringes marked.

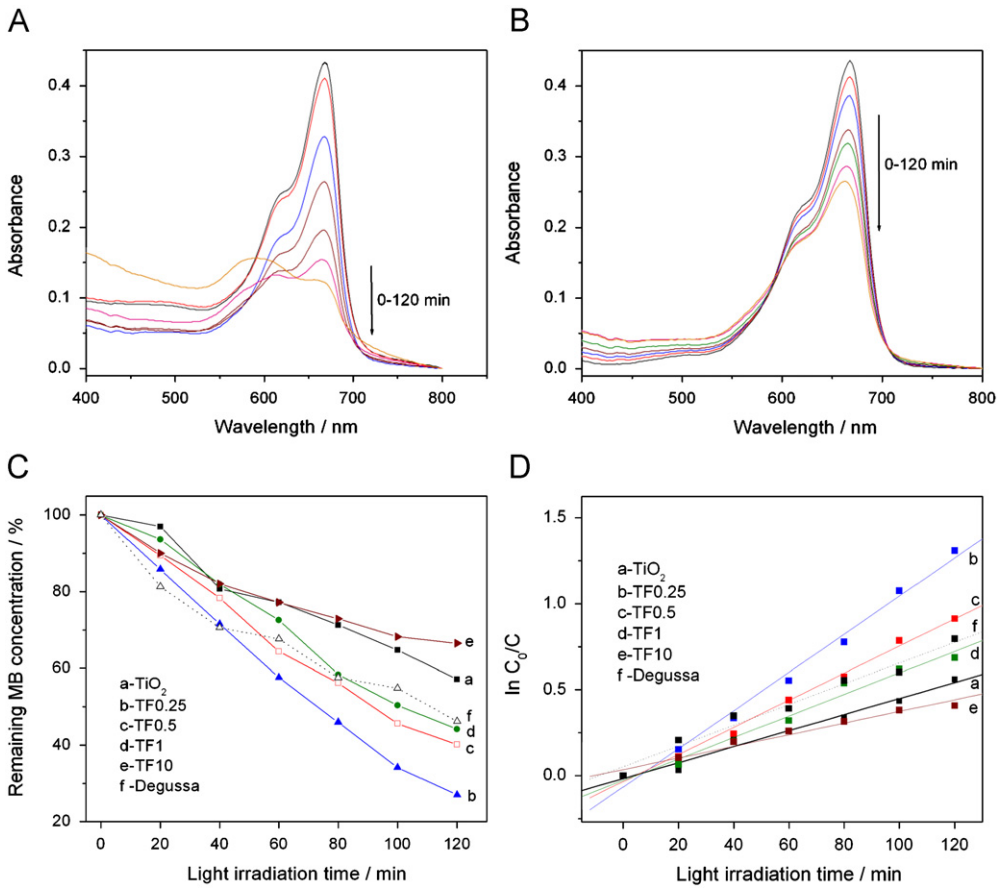

Fig. 8. Absorbance curves at time intervals 0, 20, 40, 60, 80, 100 and 120 min for (A) TF0.25, (B) pure TiO_2, both calcined at 800 °C, (C) typical variation in the normalized residual MB dye concentration as a function of visible light exposure time for the powders calcined at 800 °C and (D) the corresponding ln C_0/C vs. irradiation time graph of (C).

Table 1
Comparison of visible light photocatalytic activity of present work with some of the earlier reports.

Photocatalyst	Preparation method	Calcination temperature (°C)	Decolorization of dye		
			Dye	Decolorization (%)	Time (h)
TFe0.09	Hydrothermal	564	XRG	43	6 [40]
TFe0.5	Precipitation-hydrothermal	IR drying	Rhodamine B	90	4 [4]
N-TFe0.5	Precipitation-hydrothermal	IR drying	Rhodamine B	100	4 [4]
TFe0.5	Plasma oxidative pyrolysis	—	Methyl orange	60	2 [41]
Fe-$SrTiO_3$	Sol–gel	900	Rhodamine B	80	6 [42]
Present work	Aqueous sol–gel	800	Methylene blue	73	2

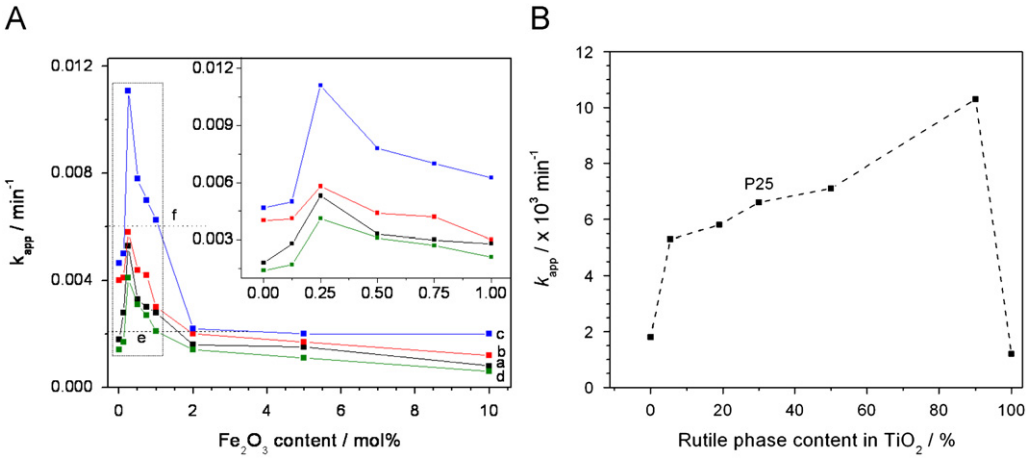

Fig. 9. (A) Rate of degradation of MB under visible light with Fe^{3+} concentration (0–10 mol%) in titania at (a) 600, (b) 700, (c) 800, (d) 900, (e) Hombikat and (f) Degussa P25. Zoomed area of k_{app} with Fe^{3+} content up to 1 mol% is illustrated in the inset. (B) Apparent first order rate constant, k_{app}, for the degradation of MB dye as a function of rutile phase content in pure and Fe^{3+} doped titania annealed at various temperatures.

samples are presented in Fig. 9. The apparent first order reaction rate constant, k_{app}, of doped titania, increased sharply with increases in Fe_2O_3 dopant concentration up to 0.25 mol% on annealing at temperatures in the range 600–900 °C. This follows a sharp decrease in k_{app} up to ~2 mol% dopant concentration followed by a plateau for titania annealed at all the temperatures.

A small increase in k_{app} is evident (Fig. 9A) as the annealing temperature of TiO_2 is increased from 600 to 800 °C at all dopant concentrations followed by a steep fall to the minimum k_{app} at 900 °C. Above 2 mol% doping, however, activity is lower than that of the pure titania at all annealing temperatures investigated. Iron(III) in small quantities behaves as electron–hole trapping centers, thus recombination of photogenerated electrons and holes are prevented, resulting in enhanced activity in the visible light region [10]. The rate of degradation of MB dye with respect to the amount of rutile phase content in the titania compositions after annealing at different temperatures are demonstrated in Fig. 9B. It is evident from the figure that, by increasing the rutile content, the photocatalytic activity has increased with a maximum k_{app} of 0.0111 min^{-1} at ~90% rutile content. This activity is higher than that of Degussa P25 titania containing ~30% rutile phase and the remaining anatase. Increasing the rutile content further to 100% reduces the activity severely, dropping to a k_{app} value of ~0.0012 min^{-1}. There are reports [44] that the optimum rutile content in titania for achieving maximum photocatalytic activity is in the range of 12–90 wt%. This long range is due to the different conditions such as method of preparation, precursors, type of dopants and heat treatment for obtaining the rutile phase.

Relatively lower activity of the heavily doped catalyst is also explained by a simple optical screening effect and the enhanced activity of TF0.25 by transferring and trapping of charges is explained in Fig. 10 as schemes. In TF0.25, the ratio of number of anatase: rutile particles is ~4:1, though it contains ~90% rutile phase (particle diameter ratio is ~1:3) and thus large number of contacts of anatase and rutile is possible. Large amount of dopant present in the system behaves as a barrier between TiO_2 particles, thus reducing the anatase–anatase and anatase–rutile contacts. High concentration of Fe^{3+} leads to the formation of an iron rich layer on the surface of the catalyst, which absorbs all of the radiation and the inner core cannot be activated properly and the trapped charges are easily getting recombined in dopant itself and the activity shows a big drop [43].

A mechanism for photocatalysis has previously been proposed [44]. The model is based on band gap variation in connected nanocrystallites as a function of size distribution and phases involved [44]. In this article, we propose a mechanism which connects the proven models for charge separation in mixed phase anatase–rutile titania and trapping of separated charges in presence of Fe^{3+} dopants. The rutile phase absorbs more light than by the anatase phase. If a rutile/anatase mixture, similar in this work (Fig. 7B, C), with higher amounts of rutile than anatase particles is exposed to light, most of the light will be absorbed by the rutile particles. The electrons could be transferred from rutile to oxygen which may result in its reduction [19]. Charge-transfer is possible through the rutile–anatase interface [44] as indicated in Fig. 7B. The electron transfer separates the charges and they are trapped by Fe^{3+} ions to form Fe^{2+} and Fe^{4+} ions which in turn enhance the e^-/h^+ lifetime in titania, as shown in the PL spectra. A synergy in energy transfer among anatase-rutile crystals by band gap variation, trapping of e^-/h^+ pairs and formation of hydroxide and super oxide radicals is represented in Fig. 10B. When all the anatase converts to rutile, contacts among similar band gap materials exist and this inhibits the activity. Therefore, an optimum quantity of rutile and Fe^{3+} is necessary to increase

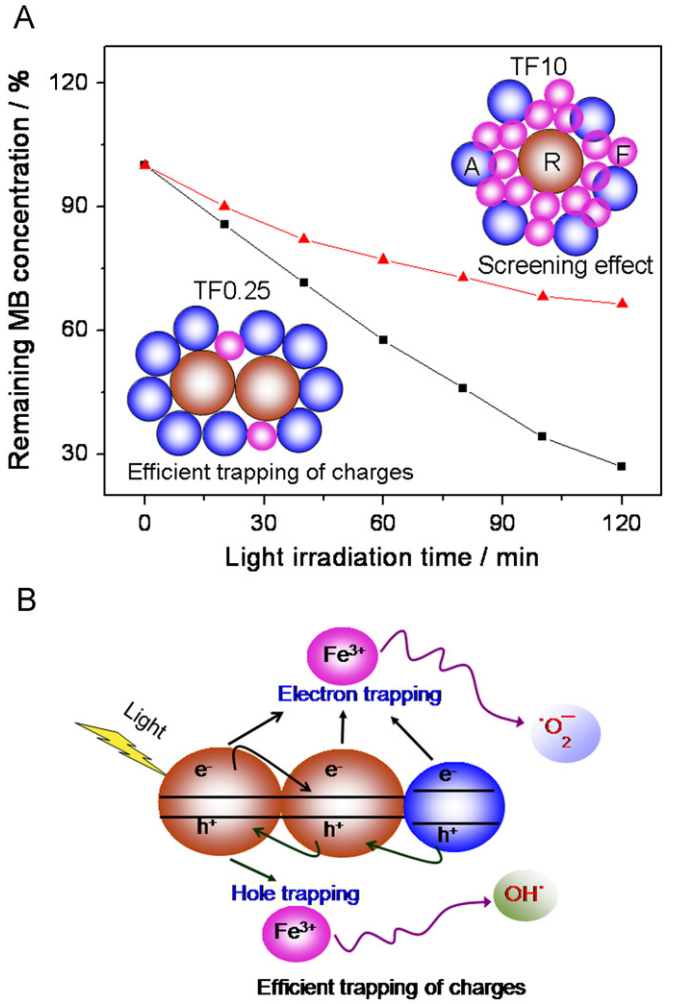

Fig. 10. (A) Model explaining the effect of optimum dopant concentration, anatase–rutile contacts and screening effect on photocatalytic activity in Fe^{3+} doped TiO_2, A, R and F represent anatase, rutile and iron(III) oxide, respectively. (B) Charge transferring and trapping model for explaining the photocatalytic activity of Fe^{3+} doped titania. A, R and F represent the anatase, rutile phases and iron(III), respectively.

the photocatalytic activity. Thus, in the present study, factors like crystallite size, surface area and porosity are less effective e^-/h^+ lifetime when determining the photocatalytic activity.

The highest activity is observed for the sample treated at 800 °C, which contains 90% of the rutile phase. Its photocatalytic activity ($k_{app}=11.1\times10^{-3}\,min^{-1}$) is higher than that of Degussa P25 ($6.03\times10^{-3}\,min^{-1}$) titania, although the contents of the rutile phase are different for the two materials. This result suggests that some synergism between anatase and rutile TiO_2 particles exists in this reaction, and that their optimal ratio depends on the sample preparation conditions. However, in the case of these samples prepared by heat treatment, the change in the crystallinity and the size of TiO_2 particles may also affect the photocatalytic activity, and it is difficult to estimate the individual contributions from each of these effects.

4. Conclusions

Visible light active nanocrystalline mesoporous Fe^{3+} doped TiO_2 photocatalyst was successfully prepared by a simple aqueous sol–gel method by using titanylsulfate and Fe(III) nitrate solutions as precursors. The Fe^{3+} doped TiO_2 powders showed a 'red-shift' in the band gap transition and thus a strong absorption in visible light region. Small levels of Fe^{3+} doping enhance the photocatalytic activity of TiO_2 in the whole range of temperatures investigated. A further increase in Fe^{3+} concentration was found to lower the phase transformation by hindering the contact between neighboring titania grains. Addition of low concentrations of Fe^{3+} ions act as photogenerated electron–hole trapping centers, while higher concentrations act as recombination centers. The optimum concentration of Fe^{3+} ions, which showed the maximum visible light activity, was 0.25 mol% at an optimum calcination temperature of 800 °C. Although what we demonstrated was the synergism between the rutile–anatase ratios in addition to the presence of Fe^{3+} for the enhanced photochemical degradation of MB, we believe that a similar effect exists in photocatalytic reactions when oxygen is used as the electron acceptor. This comprehensive study on the visible light photoactivity involving compositional variation and heat treatment of Fe^{3+} ion doped nano-titania by a sol–gel route will increase the already existing wide spectrum of applications in the degradation of hazardous industrial effluents and organic contaminants.

Acknowledgments

The authors are grateful to the Director, National Institute for Interdisciplinary Science & Technology (NIIST), CSIR, for providing the necessary facilities for the work. Mr. M. Kiran and Mr. P. Guruswamy are kindly acknowledged for their assistance in obtaining TEM and XRD data. The authors acknowledge Dr. Sarah A. Kebbell, School of Chemical Sciences, Dublin City University, Dublin 9 and Dr. Eoin Murray, IPRI, ARC (ACES), University of Wollongong, NSW, Australia, for fruitful technical discussions. One of the authors (KBJ) acknowledges CSIR for the Senior Research Fellowship.

References

[1] A. Fujishima, K. Honda, Nature 238 (1972) 37.
[2] H. Alekabi, N. Serpone, J. Phys. Chem. 92 (1988) 5726.
[3] M.R. Hoffmann, S.T. Martin, W.Y. Choi, D.W. Bahnemann, Chem. Rev. 95 (1995) 69.
[4] Y. Cong, J.L. Zhang, F. Chen, M. Anpo, D.N. He, J. Phys. Chem. C 111 (2007) 10618.
[5] D.P. Colombo, R.M. Bowman, J. Phys. Chem. 99 (1995) 11752.
[6] D.P. Colombo, K.A. Roussel, J. Saeh, D.E. Skinner, J.J. Cavaleri, R.M. Bowman, Chem. Phys. Lett. 232 (1995) 207.
[7] S. Sakthivel, H. Kisch, Angew. Chem. Int. Ed. 42 (2003) 4908.
[8] R. Asahi, T. Morikawa, T. Ohwaki, K. Aoki, Y. Taga, Science 293 (2001) 269.
[9] J.C. Yu, J.G. Yu, W.K. Ho, Z.T. Jiang, L.Z. Zhang, Chem. Mater. 14 (2002) 3808.
[10] J.C. Yu, W.K. Ho, J.G. Yu, H. Yip, P.K. Wong, J.C. Zhao, Environ. Sci. Technol. 39 (2005) 1175.
[11] S. Sato, R. Nakamura, S. Abe, Appl. Catal. A 284 (2005) 131.
[12] Y. Cao, X.T. Zhang, W.S. Yang, H. Du, Y.B. Bai, T.J. Li, J.N. Yao, Chem. Mater. 12 (2000) 3445.
[13] G. Sivalingam, K. Nagaveni, M.S. Hegde, G. Madras, Appl. Catal. B 45 (2003) 23.
[14] J.F. Zhu, Z.G. Deng, F. Chen, J.L. Zhang, H.J. Chen, M. Anpo, J.Z. Huang, L.Z. Zhang, Appl. Catal. B 62 (2006) 329.
[15] R. Priya, K.V. Baiju, S. Shukla, S. Biju, M.L.P. Reddy, K. Patil, K.G.K. Warrier, J. Phys. Chem. C 113 (2009) 6243.
[16] M.I. Litter, J.A. Navio, J. Photochem. Photobiol. A 98 (1996) 171.
[17] D. Bockelmann, M. Lindner, D. Bahnemann, Fine Part. Sci. Technol. 12 (1996) 675.
[18] W. Lee, H.S. Shen, K. Dwight, A. Wold, J. Solid State Chem. 106 (1993) 288.
[19] T. Ohno, K. Tokieda, S. Higashida, M. Matsumura, Appl. Catal. A 244 (2003) 383.
[20] H. Yamashita, M. Harada, J. Misaka, M. Takeuchi, B. Neppolian, M. Anpo, Catal. Today 84 (2003) 191.
[21] W.Y. Teoh, R. Amal, L. Madler, S.E. Pratsinis, Catal. Today 120 (2007) 203.
[22] X.Y. Li, P.L. Yue, C. Kutal, New. J. Chem. 27 (2003) 1264.
[23] S. Sivakumar, P.K. Pillai, P. Mukundan, K.G.K. Warrier, Mater. Lett. 57 (2002) 330.
[24] Y. Huang, Z.H. Ai, W.K. Ho, M.J. Chen, S. Lee, J. Phys. Chem. C 114 (2010) 6342.

[25] V.S. Smitha, K.A. Manjumol, K.V. Baiju, S. Ghosh, P. Perumal, K.G.K. Warrier, J. Sol–Gel Sci. Technol. 54 (2010) 203.
[26] J. Zhu, J. Ren, Y.N. Huo, Z.F. Bian, H.X. Li, J. Phys. Chem. C 111 (2007) 18965.
[27] J.G. Yu, X.J. Zhao, Q.N. Zhao, Mater. Chem. Phys. 69 (2001) 25.
[28] S. Ghosh, D. Divya, K.C. Remani, T.S. Sreeremya, J. Nanopart. Res. 12 (2010) 1905.
[29] M. Anpo, T. Kawamura, S. Kodama, K. Maruya, T. Onishi, J. Phys. Chem. 92 (1988) 438.
[30] K.V. Baiju, S. Shukla, K.S. Sandhya, J. James, K.G.K. Warrier, J. Phys. Chem. C 111 (2007) 7612.
[31] Y. Zhang, A.H. Yuwono, J. Wang, J. Li, J. Phys. Chem. C 113 (2009) 21406.
[32] K.N.P. Kumur, J. Engell, J. Kumar, K. Keizer, T. Okubo, M. Sadakata, J. Mater. Sci. Lett. 14 (1995) 1784.
[33] P. Nair, F. Mizukami, T. Okubo, J. Nair, K. Keizer, A.J. Burggraaf, AIChE J. 43 (1997) 2710.
[34] X.Z. Ding, X.H. Liu, J. Mater. Res. 13 (1998) 2556.
[35] W.Y. Choi, A. Termin, M.R. Hoffmann, J. Phys. Chem. 98 (1994) 13669.
[36] S. Music, M. Gotic, M. Ivanda, S. Popovic, A. Turkovic, R. Trojko, A. Sekulic, K. Furic, Mater. Sci. Eng. B 47 (1997) 33.
[37] F. Cot, A. Larbot, G. Nabias, L. Cot, J. Euro. Ceram. Soc. 18 (1998) 2175.
[38] S.M. Oh, S.S. Kim, J.E. Lee, T. Ishigaki, D.W. Park, Thin Solid Films 435 (2003) 252.
[39] A.W. Xu, Y. Gao, H.Q. Liu, J. Catal. 207 (2002) 151.
[40] J.F. Zhu, W. Zheng, H.E. Bin, J.L. Zhang, M. Anpo, J. Mol. Catal. A 216 (2004) 35.
[41] X.H. Wang, J.G. Li, H. Kamiyama, Y. Moriyoshi, T. Ishigaki, J. Phys. Chem. B 110 (2006) 6804.
[42] T.H. Xie, X. Sun, J. Lin, J. Phys. Chem. C 112 (2008) 9753.
[43] K.T. Ranjit, B. Viswanathan, J. Photochem. Photobiol. A 108 (1997) 79.
[44] A. Zachariah, K.V. Baiju, S. Shukla, K.S. Deepa, J. James, K.G.K. Warrier, J. Phys. Chem. C 112 (2008) 11345.